

The two-dimensional kinetic ballooning theory for trapped electron mode in tokamak

Cite as: Phys. Plasmas **26**, 022503 (2019); <https://doi.org/10.1063/1.5048538>

Submitted: 16 July 2018 . Accepted: 15 January 2019 . Published Online: 04 February 2019

T. Xie , Y. Z. Zhang, S. M. Mahajan , F. Wu, Hongda He, and Z. Y. Liu



View Online



Export Citation



CrossMark

ARTICLES YOU MAY BE INTERESTED IN

[Full-f gyrokinetic simulation of turbulence in a helical open-field-line plasma](#)

Phys. Plasmas **26**, 012307 (2019); <https://doi.org/10.1063/1.5074179>

[Electromagnetic effect on geodesic acoustic mode with adiabatic electrons](#)

Phys. Plasmas **26**, 022506 (2019); <https://doi.org/10.1063/1.5080271>


[Effect of toroidal rotation on the linear stability of drift-resistive-inertial ballooning modes](#)

Phys. Plasmas **26**, 022504 (2019); <https://doi.org/10.1063/1.5079596>



NEW!

Sign up for topic alerts
New articles delivered to your inbox



The two-dimensional kinetic ballooning theory for trapped electron mode in tokamak

Cite as: Phys. Plasmas **26**, 022503 (2019); doi: [10.1063/1.5048538](https://doi.org/10.1063/1.5048538)

Submitted: 16 July 2018 · Accepted: 15 January 2019 ·

Published Online: 4 February 2019



View Online



Export Citation



CrossMark

T. Xie,^{1,a)}  Y. Z. Zhang,² S. M. Mahajan,³  F. Wu,^{1,a)} Hongda He,⁴ and Z. Y. Liu⁵

AFFILIATIONS

¹Department of Physics, Sichuan University of Science & Engineering, Zigong, Sichuan 643000, China

²Center for Magnetic Fusion Theory, CAS, Hefei, Anhui 230026, China

³Institute for Fusion Studies, University of Texas at Austin, Austin, Texas 78712, USA

⁴Southwestern Institute of Physics, P.O. Box 432, Chengdu, Sichuan 610041, China

⁵Department of Modern Physics, University of Science and Technology of China, Hefei, Anhui 230026, China

^{a)}Authors to whom correspondence should be addressed: xietao@ustc.edu.cn and fei.wu.cn@163.com

ABSTRACT

The two-dimensional (2D) kinetic theory for a collisionless trapped electron mode is developed based on the Fourier-ballooning transform in an up-down symmetric equilibrium (illustrated via concentric circular magnetic surfaces). The system consists of two equations: the ballooning (integral) equation with a parameterized Floquet phase and a second order differential equation for the distribution of the Floquet phase. The coupled equations are, then, numerically solved as an eigenvalue problem yielding the 2D mode structure (in real space) as well as the global (phase-independent) eigenvalue for an L-mode parameter set. The 2D mode structure exhibits apparent radial-poloidal asymmetry; due to the poloidal coupling, the radial correlation length is found to be, at least, twice as large as the poloidal one. The global (phase-independent) eigenvalue of the mode differs considerably from the conventional local (phase-dependent) estimate. This paper shares many technical aspects with a published paper that works out the 2D kinetic theory for the ion temperature gradient mode [Xie et al., Phys. Plasmas **24**, 102506 (2017)].

Published under license by AIP Publishing. <https://doi.org/10.1063/1.5048538>

I. INTRODUCTION

It is generally believed that trapped electron modes (TEMs) are one of the leading candidates behind the drift wave turbulence, responsible for the anomalous electron transport in the tokamak operation in the L-mode.¹ Until now, calculating the mode frequency/growth rate has been the principal objective of most linear theories,^{2–11} even though the significance of the mode structure was definitively realized since it is needed for correctly calculating the Reynolds stress—the driving force generating the shear flow for turbulence suppression. It is important to point out that the mode structure is not accessible in the typical conventional or one-dimensional (1D) ballooning theory,^{12–15} devised to approximately capture the effects of toroidicity on linear modes in a torus like tokamak. A few years ago, however, a 2D ballooning theory was deliberately constructed, known as weakly (up-down) asymmetric ballooning theory (WABT)—first in a fluid^{16,17} and then in a kinetic model¹⁸ for ion temperature gradient (ITG) eigenmodes. The 2D ballooning

structure was then transformed back to obtain the mode structure in physical space which was, in turn, used to derive a reliable analytical expression for Reynolds stress (see Ref. 19 for the fluid model). The advent of the concept “zonal flow-drift wave system”^{20–22} throws out new challenges, for instance, the need for using the valid mode structure for correctly calculating group velocities that transport drift-wave energy. It was shown in Ref. 22 that it is the sharp edge of radial group velocity that triggers a pair of “cavitons” decaying into many “instantons,” indicating the inappropriateness of using Fourier representation for describing group velocities. Whether or not such a pattern remains valid for zonal flow induced by TEM—a mode propagating in the electron diamagnetic direction—is the major motivation behind developing the present 2D TEM theory.

The interested readers may find a brief history of the development of ballooning theories in the introduction of Ref. 17. We would also like to share our perspective on the significance and methodology of the ballooning theory used in the

present paper. As an asymptotic theory in a high n (toroidal mode number) limit, the ballooning theory was developed to deal with local modes, mostly, in the drift wave frequency range. These modes were thought to be responsible for the observed micro-turbulence (leading to anomalous transport) in tokamaks. The magnetic shear in a tokamak setting has a crucial impact on the drift wave, because away from the rational surface, the parallel wave number becomes large resulting in strong (the so-called shear) stabilization^{23,24} and radial localization of the mode. It is precisely the origin of the “natural” boundary condition issue to be discussed soon. The “natural” boundary condition for numerical simulation of local modes must be determined by the asymptotic solution of the wave equation for sufficiently large radii, e.g., the outgoing wave boundary condition invoked for the slab model drift waves.²⁵ For a 2D system like tokamak, however, this exercise of finding the natural boundary conditions is totally non-trivial as analyzed in Sec. IV of Ref. 17, where the issue is finally resolved by making use of the 2D ballooning theory for ITG in the fluid model. For the ITG, the weakly asymmetric ballooning theory (WABT) structure was chosen among the four flavors mentioned in Ref. 17. We choose the same model for TEM in this paper, because WABT is likely to be the most relevant for anomalous electron transport in low mode regimes. The methodology used in the present paper is based on the 2D Fourier-ballooning transform (with a unique inverse) that is a direct extension of Lee-Van Dam representation as explained in Sec. II D. The 2D ballooning space is spanned by two physical quantities: the Fourier image of parallel wave number k and Floquet phase λ . To the leading order, the ballooning equation is “solved” with the Floquet phase as a (yet to-be-determined) parameter. Such a parameterized solution is then used to construct the equation of the second dimension for the Floquet phase distribution (FPD) $\psi(\lambda)$. The task for a complete solution of the wave function in 2D ballooning space $\varphi(\mathbf{k}, \lambda) = \psi(\lambda)\chi(\mathbf{k}, \lambda)$ is accomplished in the present paper by an iterative algorithm to achieve convergence. This is precisely the same methodology used in Ref. 18 for the kinetic ITG mode. The interested readers may refer to Eqs. (1)–(5) in Ref. 18 to get further information. For those who may wonder what distinguishes the results of Ref. 17 from Ref. 18 (the former takes a simple analytical model for potential in the Floquet phase equation while the latter did not), we shall provide more comprehensive information in a future publication since this manuscript pertains to TEM, not to ITG.

Although the 2D ITG linear theory was developed for both the fluid and the kinetic models, the 2D TEM theory in this paper is based, solely, on a kinetic model. When the mode frequency falls in the range much lower than the electron bounce frequency, one ought to consider the driving force from trapped electrons arising from the magnetic drift resonance. In this paper, we focus on the collisionless branch of TEM that pertains when the collision frequency is much smaller than the electron magnetic drift frequency. For the resonant TEM, then, the mode frequency ω is on the order of the magnetic drift frequency, and the phase velocity is in the direction of electron diamagnetic drift. In Sec. II, we begin with the electron drift kinetic equation to derive the non-adiabatic density response of the trapped

electron in 2D configuration space for the bounce frequency larger than the mode frequency (Sec. II A). The density perturbation is, then, cast into ballooning representation using a 2D inverse Fourier-ballooning transform (Sec. II B). Since the mode frequency of TEM is much less than the transit frequency of the passing electron (Landau resonance to the passing electron is absent), it is reasonable to take the passing electron response as adiabatic. In fact, the collisionless TEM is a reactive mode and does NOT require dissipation for destabilization. The perturbed passing ion density can be derived from gyro-kinetic equation as presented in Ref. 18, while the effect of the trapped ion is neglected. As a result, the 2D eigenmode equation for collisionless weakly up-down asymmetric TEM is obtained from the quasi-neutrality condition (Sec. II C). The lowest order equation is an integral equation with a parameterized Floquet phase, while the higher order equation for the distribution of the Floquet phase is a differential equation, containing all translational symmetry breaking (TSB) terms up to the second order, derived in the same procedure as that used for the 2D kinetic ITG mode.¹⁸ In subsection II D, the existing TEM kinetic theories based on 1D ballooning theory are compared to the 2D theory developed in this paper. The 2D system is solved numerically for the global eigenvalue and the 2D mode structure in Sec. III by making use of the same numerical algorithm as in Ref. 18. Major conclusions of this paper are summarized in Sec. IV. Appendix A shows the derivation of the non-adiabatic trapped electron density response for large bounce frequency based on the electron drift kinetic equation in real space. In Appendix B, the analytical expression of higher order TSB terms is explicitly provided.

II. THE WEAKLY UP-DOWN ASYMMETRIC TEM

A. Electron density response to TEM in the physical configuration

The collisionless TEM model of this paper is built on a large-aspect-ratio, up-down symmetric tokamak equilibrium with concentric circular magnetic surfaces. In the toroidal coordinates (r, ϑ, ζ) corresponding to the radial, poloidal, and toroidal directions, respectively, the electron drift kinetic equation is²⁶

$$(\omega - \hat{\omega}_{de} + iv_{\parallel} \mathbf{b} \cdot \nabla) h(r, \vartheta, \zeta; v_{\parallel}, v_{\perp}) = -F_M(\omega - \hat{\omega}_{*T}) \varphi(r, \vartheta, \zeta), \quad (1)$$

where $h(r, \vartheta, \zeta; v_{\parallel}, v_{\perp})$ is the non-adiabatic perturbed distribution function of the electron guiding center and ω , $\hat{\omega}_{de} \equiv (2iT_e/eBR)(\hat{v}_{\parallel}^2 + \hat{v}_{\perp}^2/2)[\sin \vartheta(\partial/\partial r) + (\cos \vartheta/r)(\partial/\partial \vartheta)]$, and $\hat{\omega}_{*T} = (iT_e q(r)/eBL_n r)[1 + \eta_e(\hat{v}^2 - 3/2)](\partial/\partial \zeta)$ are the mode, the toroidal drift, and the diamagnetic frequencies, respectively. In Eq. (1), $\hat{v}_{\parallel} \equiv v_{\parallel}/v_{te}$, $\hat{v}_{\perp} \equiv v_{\perp}/v_{te}$, $v_{te} \equiv \sqrt{2T_e/m_e}$, $\mathbf{b} \cdot \nabla = (1/q(r)R)[\partial/\partial \vartheta + q(r)\partial/\partial \zeta]$, $\hat{v}^2 = \hat{v}_{\perp}^2 + \hat{v}_{\parallel}^2$, $F_M \equiv (\pi v_{te}^2)^{-3/2} \exp(-\hat{v}_{\parallel}^2 - \hat{v}_{\perp}^2)$, $\eta_e \equiv L_n/L_{Te}$, $L_n \equiv -(d \ln n_e/dr)_r^{-1}$, $L_{Te} \equiv -(d \ln T_e/dr)_r^{-1}$, $n_e(r)$ is the electron density in equilibrium, $T_e(r)$ is the electron temperature, $q(r)$ is the safety factor, \mathbf{b} is the unit vector of magnetic field, e is the unit charge, m_e is the electron mass, $v_{\parallel} = \sigma \sqrt{4\mu B_0 \varepsilon(r)/m_e} \sqrt{\kappa^2 - \sin^2(\vartheta/2)}$, $\mu = m_e v_{\perp}^2/2B$ is the magnetic moment, $\sigma \equiv \text{sgn}(v_{\parallel})$, $\varepsilon(r) \equiv r/R$, $\kappa^2 \equiv \sin^2(\vartheta_r/2)$, and ϑ_r is

the poloidal angle of the turning point where $v_{\parallel} = 0$. The perturbed electrostatic potential $\varphi(r, \vartheta, \zeta)$ is normalized (to T_e/e), and $B \approx B_0$ and $R \approx R_0$ are the magnetic field and major radius of the magnetic axis, respectively.

For an axisymmetric tokamak, the mode reduces to a single toroidal number n , $\varphi(r, \vartheta, \zeta) = \varphi_n(r, \vartheta)e^{in\zeta}$, $h(r, \vartheta, \zeta; v_{\parallel}, v_{\perp}) = h_n(r, \vartheta; v_{\parallel}, v_{\perp})e^{in\zeta}$, and $\mathbf{b} \cdot \nabla \rightarrow (1/q(r)R)[\partial/\partial\vartheta + inq(r)]$.

For large bounce frequency ($\omega_{be} \equiv \sqrt{\varepsilon}v_{te}/qR > \omega$), the dimensionless non-adiabatic density response of the trapped electron $\hat{n}_{te}(r, \vartheta)$ in real space can be derived from Eq. (1) as shown in Appendix A

$$\hat{n}_{te}(r, \vartheta) = -e^{-inq(r)\vartheta} \int dv^3 F_M \frac{\omega - \hat{\omega}_{*T}}{\omega - \langle \omega_{de} \rangle \hat{v}^2} \langle e^{inq(r)\vartheta} \varphi_n(r, \vartheta) \rangle. \quad (2)$$

For a high n local mode pertaining to a given rational surface r_j , the monotonic safety factor $q(r)$ can be expanded up to the first order, as $q(r) \approx q(r_j) + (dq/dr)(r - r_j) \equiv q(r_j) + x/n$. Then, substituting

$$\varphi_n(x, \vartheta) \equiv \exp(-im\vartheta) \sum_l \varphi_l(x) \exp(-il\vartheta) \quad (3)$$

into $\langle e^{inq(r)\vartheta} \varphi_n(r, \vartheta) \rangle$ yields

$$\langle e^{inq(r)\vartheta} \varphi_n(r, \vartheta) \rangle \approx \langle e^{i(m+x)\vartheta} \varphi_n(r, \vartheta) \rangle = \left\langle e^{ix\vartheta} \sum_l e^{-il\vartheta} \varphi_l(x) \right\rangle, \quad (4)$$

where $\varphi_l(x)$ is known as the wave function in (x, l) representation, $x \equiv nq(r_j)\hat{s}(r - r_j)/r_j$, $m = nq(r_j)$ is an integer denoting the poloidal mode number, and the integer l labels the sidebands coupled to the central Fourier mode m .

B. Electron density response to TEM in 2D Fourier-ballooning representation

By making use of the 2D Fourier-ballooning transform, we get^{16,17,27,28}

$$\varphi_l(x) = \frac{1}{2\pi} \int_{-\pi}^{\pi} d\lambda \int_{-\infty}^{+\infty} dk e^{ik(x-l) - i\lambda l} \varphi(k, \lambda), \quad (5)$$

with $\varphi(k, \lambda) := \psi(\lambda)\chi(k, \lambda)$ and the Poisson formula

$$\sum_l e^{-il(\vartheta+k+\lambda)} = 2\pi \sum_p \delta(2p\pi - \vartheta - k - \lambda), \quad (6)$$

Equation (4) becomes (in the 2D ballooning representation)

$$\left\langle e^{ix\vartheta} \sum_l e^{-il\vartheta} \varphi_l(x) \right\rangle = 2\pi \oint d\lambda \psi(\lambda) \sum_p e^{ix(2p\pi - \lambda)} \langle \chi(2p\pi - \vartheta - \lambda, \lambda) \rangle, \quad (7)$$

where $\chi(k, \lambda)$ is the ballooning wave function with a parameterized Floquet phase λ and $\psi(\lambda)$ is the FPD mentioned in the Introduction.

Substituting Eq. (7) into Eq. (2) yields

$$\hat{n}_{te}(r, \vartheta) = -2\pi e^{-inq(r)\vartheta} \int dv^3 F_M \frac{\omega - \hat{\omega}_{*T}}{\omega - \langle \omega_{de} \rangle \hat{v}^2} \oint d\lambda \psi(\lambda) \times \sum_p e^{ix(2p\pi - \lambda)} \langle \chi(2p\pi - \vartheta - \lambda, \lambda) \rangle. \quad (8)$$

For the trapped electron, the integral over velocity space can be reduced to the integral over κ^2 and \hat{v}^2

$$\int dv^3 F_M(\dots) = \sqrt{\frac{2\varepsilon(r)}{\pi}} \int_0^{\infty} d\hat{v}^2 \hat{v} e^{-\hat{v}^2} \int_{\kappa_{\min}^2}^1 \frac{d\kappa^2}{\sqrt{\kappa^2 - \sin^2(\vartheta/2)}} (\dots), \quad (9)$$

where $\kappa_{\min}^2 \equiv \sin^2(\vartheta/2)$. Apparently, Eq. (8) has two poloidal scales: the fast scale of the exponential term $\exp(-inq(r)\vartheta)$ and the slow one contained in the integral over velocity space. Substituting Eq. (9) into Eq. (8) yields

$$\hat{n}_{te}(r, \vartheta) = -e^{-inq(r)\vartheta} \sqrt{\frac{2\varepsilon(r)}{\pi}} \int_{\kappa_{\min}^2}^1 \frac{d\kappa^2}{\sqrt{\kappa^2 - \sin^2(\vartheta/2)}} \Phi(x, \kappa^2) \times \int_0^{\infty} d\hat{v}^2 \hat{v} e^{-\hat{v}^2} \frac{\omega - \hat{\omega}_{*T}}{\omega - \langle \omega_{de} \rangle \hat{v}^2}, \quad (10)$$

where

$$\Phi(x, \kappa^2) = 2\pi \oint d\lambda \psi(\lambda) \sum_p e^{ix(2p\pi - \lambda)} \langle \chi(2p\pi - \vartheta - \lambda, \lambda) \rangle. \quad (11)$$

For further analysis, it is useful to define

$$\hat{I}(\zeta_e) \equiv - \int_0^{\infty} d\hat{v}^2 \hat{v} e^{-\hat{v}^2} \frac{\omega - \hat{\omega}_{*T}}{\omega - \langle \omega_{de} \rangle \hat{v}^2} = \sqrt{\pi} \zeta_e^2 \left\{ (1 + \zeta_e Z(\zeta_e)) \left(1 - \frac{\omega_{*e}}{\omega} \right) + \eta_e \frac{\omega_{*e}}{\omega} \left[1 - \zeta_e^2 + \zeta_e Z(\zeta_e) \left(\frac{3}{2} - \zeta_e^2 \right) \right] \right\}, \quad (12)$$

where $\zeta_e^2 \equiv \omega/\langle \omega_{de} \rangle$ is a function of r and κ^2 and $Z(\zeta_e) \equiv (1/\sqrt{\pi}) \int_L d\hat{v} \exp(-\hat{v}^2)/(\hat{v} - \zeta_e)$ is the plasma dispersion function. Then, Eq. (10) becomes

$$\hat{n}_{te}(r, \vartheta) = \sqrt{\frac{2\varepsilon(r)}{\pi}} e^{-inq(r)\vartheta} \int_{\kappa_{\min}^2}^1 \frac{d\kappa^2}{\sqrt{\kappa^2 - \sin^2(\vartheta/2)}} \Phi(x, \kappa^2) \hat{I}(\zeta_e). \quad (13)$$

Now, it is straightforward to convert the density response in real space to the 2D ballooning representation by making use of the inverse Fourier-ballooning transform.

Combining Eqs. (3) and (5) results in

$$\hat{n}_{te}(x, \vartheta) = e^{-im\vartheta} \sum_l \hat{n}_{te,l}(x) e^{-il\vartheta} = e^{-im\vartheta} \sum_l e^{-il\vartheta} \oint d\lambda \int_{-\infty}^{\infty} dk e^{ik(x-l) - i\lambda l} \hat{n}_{te}(k, \lambda). \quad (14)$$

Use is made of Eq. (14) to replace LHS of Eq. (13), leading to

$$\sum_l e^{-il\vartheta} \oint d\lambda \int_{-\infty}^{\infty} dk e^{ik(x-l) - i\lambda l} \hat{n}_{te}(k, \lambda) = \sqrt{\frac{2\varepsilon(r)}{\pi}} e^{-ix\vartheta} \int_{\kappa_{\min}^2}^1 \frac{d\kappa^2}{\sqrt{\kappa^2 - \sin^2(\vartheta/2)}} \Phi(x, \kappa^2) \hat{I}(\zeta_e). \quad (15)$$

Multiplying $e^{-ik'x}$ on both sides of Eq. (15) and integrating over the fast variable x , one obtains

$$\begin{aligned}
 & \sum_{\Gamma} e^{-i\vartheta} \oint d\lambda e^{-i(k+\lambda)l} \hat{n}_{te}(k, \lambda) \\
 &= 2\pi \sqrt{\frac{2\varepsilon(r)}{\pi}} \int_{\kappa_{\min}^2}^1 \frac{d\kappa^2}{\sqrt{\kappa^2 - \sin^2 \frac{\vartheta}{2}}} \\
 & \quad \times \oint d\lambda \psi(\lambda) \hat{I}(\zeta_e) \sum_p \langle \chi(2p\pi - \vartheta - \lambda, \lambda) \rangle \delta(2p\pi - \vartheta - \lambda - k).
 \end{aligned} \tag{16}$$

The slow radial variable r is not under integration over x . Such terms can be split into two parts: $r - r_j \sim x/n = (x-l)/n + l/n$. The first $(x-l)/n$ is a small correction to the ballooning equation at higher order ($1/n$), which can be neglected. The second part proportional to l/n breaks the translational symmetry. Since it is the translational symmetry that allowed us to convert a 2D problem into an effective 1D system, its breaking, necessarily, forces us into dealing with the second dimension [see Eq. (21)].

Integrating Eq. (16) over ϑ yields (using the delta function)

$$\begin{aligned}
 \oint d\lambda \hat{n}_{te}(k, \lambda) &= \sqrt{\frac{2\varepsilon(r)}{\pi}} \oint d\lambda \psi(\lambda) \int_{\kappa_{\min}^2}^1 \frac{d\kappa^2}{\sqrt{\kappa^2 - \sin^2 \frac{(k+\lambda)}{2}}} \hat{I}(\zeta_e) \\
 & \quad \times \sum_p \langle \chi(2p\pi - \vartheta - \lambda, \lambda) \rangle.
 \end{aligned} \tag{17}$$

The dimensionless non-adiabatic density response of the trapped electron in 2D Fourier-ballooning representation is identified to be

$$\begin{aligned}
 \hat{n}_{te}(k, \lambda) &= \sqrt{\frac{2\varepsilon(r)}{\pi}} \int_{\kappa_{\min}^2}^1 \frac{d\kappa^2}{\sqrt{\kappa^2 - \sin^2 \frac{(k+\lambda)}{2}}} \hat{I}(\zeta_e) \psi(\lambda) \\
 & \quad \times \sum_p \langle \chi(2p\pi - \vartheta - \lambda, \lambda) \rangle.
 \end{aligned} \tag{18}$$

C. TEM eigen-equations

Since the mode frequency of TEM is greater than the ion bounce frequency, only passing ions are retained. The corresponding non-adiabatic density response has been derived as shown in Eq. (9) of Ref. 18. The passing electron response is assumed to be adiabatic. The quasi-neutrality then yields the integral TEM eigen-equation in Fourier-ballooning representation

$$\begin{aligned}
 & \int_{-\infty}^{\infty} dk' K(k, k', \lambda, \lambda) \varphi(k', \lambda) - \frac{1 + \tau_{e0}}{1 + \tau_e} \sqrt{\frac{2\varepsilon(r)}{\pi}} \frac{\omega}{\omega_{*e0}} \psi(\lambda) \\
 & \quad \times \int_{\kappa_{\min}^2}^1 \frac{d\kappa^2}{\sqrt{\kappa^2 - \sin^2 \frac{(k+\lambda)}{2}}} \hat{I}(\zeta_e) \sum_p \langle \chi(2p\pi - \vartheta - \lambda, \lambda) \rangle = \Omega \varphi(k, \lambda),
 \end{aligned} \tag{19}$$

where $\lambda \equiv (-i/m)(\partial/\partial\lambda)$, $\tau_e \equiv T_e(r)/T_i(r)$, $T_i(r)$ is the ion temperature, the quantities with subscript "0" stand for the values at rational surface r_j , e.g., $\omega_{*e0} \equiv k_{\vartheta} T_e(r_j)/eBL_n(r_j)$ with $k_{\vartheta} \equiv -nq(r_j)/r_j$, the integral kernel $K(k, k', \lambda, \lambda)$ is defined by Eq. (11) in Ref. 18 (not repeated here), and

$$\Omega \equiv (1 + \tau_{e0}) \frac{\omega}{\omega_{*e0}} \tag{20}$$

is the global (Floquet phase-independent) eigenvalue. In the derivation, use is made of linear density and temperature profiles, $n_s(r) := n_s(r_j)(1 - t_n x/m)$ ($s = i, e$), $T_s(r) := T_s(r_j)(1 - t_{Ts} x/m)$ with $t_n \equiv r_j/\delta L_{n0}$, $t_{Ts} \equiv r_j/\delta L_{Ts0}$, $L_{n0} \equiv L_n(r_j) = -(d \ln n_i / dr)_{r_j}^{-1}$, and $L_{Ts0} \equiv L_{Ts}(r_j) = -(d \ln T_s / dr)_{r_j}^{-1}$.

Equation (19) is the full 2D integro-differential equation in (k, λ) representation. The WABT is to seek solution satisfying $1/n \ll |\lambda \ln \psi(\lambda)| \ll 1$ by expanding Eq. (19) to the second order of λ .¹⁶⁻¹⁹ The procedure followed here is the same as that used in Ref. 18. The integral kernel $K(k, k', \lambda, \lambda)$ provides all TSB terms for the passing ion as presented in Ref. 18. For the trapped electron, all TSB terms are contained in the product

$$g(\kappa, \lambda) \equiv \frac{1 + \tau_{e0}}{1 + \tau_e} \sqrt{\frac{2\varepsilon(r)}{\pi}} \left(\frac{\omega}{\omega_{*e0}} \hat{I}(\zeta_e) \right). \tag{21}$$

The Taylor expansion of Eq. (21) (up to the second order) yields

$$g(\kappa, \lambda) = g(\kappa, 0) + \left. \frac{dg(\kappa, \lambda)}{d\lambda} \right|_{\lambda=0} \lambda + \frac{1}{2} \left. \frac{d^2 g(\kappa, \lambda)}{d\lambda^2} \right|_{\lambda=0} \lambda^2. \tag{22}$$

For the sake of readability, the coefficients of Eq. (22) will be put in Appendix B.

Substituting Eq. (22) into Eq. (19), we obtain the following system likewise in Sec. II of Ref. 18:

$$[L_0 - \Omega(\lambda)] \chi(k, \lambda) = 0 \tag{23}$$

and

$$\left[\frac{d^2}{d\lambda^2} + \frac{i n \bar{L}_1}{\bar{L}_2} \frac{d}{d\lambda} + \frac{n^2}{\bar{L}_2} (\Omega(\lambda) - \Omega) \right] \psi(\lambda) = 0 \quad (n \equiv |n|), \tag{24}$$

where

$$\begin{aligned}
 L_0 \chi(k, \lambda) &= \int_{-\infty}^{\infty} dk' K(k, k', \lambda, 0) \chi(k', \lambda) \\
 & \quad - \int_{\kappa_{\min}^2}^1 d\kappa^2 g(\kappa, 0) \bar{\Phi}(k, \lambda, \kappa^2),
 \end{aligned} \tag{25}$$

$$\Omega(\lambda) \equiv (1 + \tau_{e0}) \frac{\omega(\lambda)}{\omega_{*e0}}, \tag{26}$$

$$\begin{aligned}
 \bar{L}_1(\lambda) &= -\frac{1}{q_0} \frac{1}{\int_{-\infty}^{\infty} dk \chi^*(k, \lambda) \chi(k, \lambda)} \int_{-\infty}^{\infty} dk \chi^*(k, \lambda) \\
 & \quad \times \left[\int_{-\infty}^{\infty} dk' \frac{dK}{d\lambda} \Big|_{\lambda=0} \chi(k', \lambda) - \int_{\kappa_{\min}^2}^1 d\kappa^2 \frac{dg(\kappa, \lambda)}{d\lambda} \Big|_{\lambda=0} \bar{\Phi}(k, \lambda, \kappa^2) \right],
 \end{aligned} \tag{27}$$

$$\begin{aligned}
 \bar{L}_2(\lambda) &= -\frac{1}{2q_0^2} \frac{1}{\int_{-\infty}^{\infty} dk \chi^*(k, \lambda) \chi(k, \lambda)} \int_{-\infty}^{\infty} dk \chi^*(k, \lambda) \left[\int_{-\infty}^{\infty} dk' \frac{d^2 K}{d\lambda^2} \Big|_{\lambda=0} \right. \\
 & \quad \times \chi(k', \lambda) - \left. \int_{\kappa_{\min}^2}^1 d\kappa^2 \frac{d^2 g(\kappa, \lambda)}{d\lambda^2} \Big|_{\lambda=0} \bar{\Phi}(k, \lambda, \kappa^2) \right],
 \end{aligned}$$

with

$$\bar{\Phi}(k, \lambda, \kappa^2) \equiv \frac{1}{\sqrt{\kappa^2 - \sin^2 \frac{(k + \lambda)}{2}}} \sum_p \langle \chi(2p\pi - \vartheta - \lambda, \lambda) \rangle. \quad (29)$$

Equation (23) is known as the Floquet phase parameterized 1D ballooning equation. Equation (24), a second order differential equation, can be called as the FPD equation. The two equations constitute the basic framework for weakly up-down asymmetric ballooning theory.

It is noticeable that Eq. (23) is invariant under the combined parity inversion ($k \rightarrow -k, \lambda \rightarrow -\lambda$). Therefore, the local eigenvalue $\Omega(\lambda)$ and $\bar{L}_1(\lambda)$ and $\bar{L}_2(\lambda)$ are even functions of λ .

D. Remarks on the relationship to conventional ballooning theory

Various conventional ballooning theories^{12–15} share two common features: (a) the mode eigenvalue is determined by the (1D) ballooning equation, the contribution from (the 2nd dimension) higher order is neglected, and (b) the Floquet phase (λ in Ref. 12 and η_0 in Ref. 13) is 0 or π , leading to the up-down symmetric mode structure in up-down symmetric equilibrium. This prescription encounters a solvability issue: the solution is valid only in very special situations^{27,29} for a (non-ideal) complex system. In fact, the solvability constraint may be satisfied only at some isolated radial positions (the phrase *isolated modes* was coined in Ref. 30); such mode structures lead to insignificant transport.

In the past 40 years, the linear theories for TEM have been essentially based on the conventional ballooning theory, in fact, limited to seek the solution of the 1D ballooning equation alone with zero (or π) Floquet phase (the so-called quasi-mode by some authors^{2–11,31,32}). Since the mode structure is up-down symmetric, it yields zero Reynolds stress. There have been some attempts to identify the radial correlation length to be associated with a finite Floquet phase; however, the description remains quite incomplete. The ambiguous 2D mode structure in conventional ballooning theories is not conducive to a plausible calculation of the group velocities of TEM energy transport.

In contrast, the 2D Fourier-ballooning transform^{27,28} adopted in this paper [an extension of Lee-Van Dam (1D) representation¹²] does lead us to a dependable 2D mode structure. This theory does rely on the fact that to the leading order, the system has translational symmetry (this realization is what led to the 1D ballooning theory of Lee-Van Dam¹²). Although the leading order system is invariant under the transform $x \rightarrow x + 1, l \rightarrow l + 1$, it is the breakdown of this symmetry that compels a 2D structure in the ballooning space, i.e., the Floquet phase is no longer a fixed parameter (as in the conventional 1D approach) and becomes a variable. The TSB terms (functions of x and/or l but not of $x - l$) in the (x, l) representation, collectively, create the basis for the higher order 2D theory.

In the 2D Fourier-ballooning theory, the isolated mode morphs into a WABT mode.^{16–18} By introducing a second small parameter, WABT relaxes the rigorous solvability condition for the isolated mode; the result is a weakly up-down asymmetric mode structure causing a finite residual Reynolds stress (as calculated in Ref. 19) to drive zonal flow and saw-tooth like behavior in the radial group velocity (in Ref. 22). In addition to this

qualitative change, the higher order (from the 2nd dimension terms) contribution to eigenvalue is, generally, not negligible; this is indeed true for the examples worked out in this paper.

III. NUMERICAL RESULTS

An iterative integral code [TEM-WABT] was developed to solve the coupled system consisting of the ballooning (integral) equation (23) and the FPD equation (24). Equation (23) is solved numerically by making use of the spectral method based on Weber-Hermite functions. The ballooning wave function, then, is approximated by

$$\chi(k, \lambda) \approx \sum_{j=0}^N A_j(\lambda) H_j(k) \exp(-k^2/2), \quad (30)$$

where $H_j(k)$ is the Hermite polynomial of degree j and $A_j(\lambda)$ is the function of λ to be determined.

By multiplying $H_{j'}(k) \exp(-k^2/2)$ ($j' = 0, 1, \dots, N$) and integrating over k , Eq. (23) [with Eq. (25)] is converted into a system of linear algebraic equations

$$[\mathbf{M} - \Omega(\lambda)\mathbf{I}]\mathbf{A} = 0, \quad (31)$$

where $\mathbf{A} \equiv (A_0, A_1, \dots, A_N)^T$, \mathbf{M} is a $(N + 1) \times (N + 1)$ dimensional matrix and \mathbf{I} is the unit matrix. The integrations over τ, k', κ^2 , and ϑ are performed with a Gaussian rule of even order. The integration over k is carried out with a trapezoidal rule. In the calculation, 5 bounce harmonics are kept for trapped electrons ($p = -2$ through $p = 2$). The same numerical integral scheme is also used to calculate $\bar{L}_1(\lambda)$ and $\bar{L}_2(\lambda)$.

Since the matrix \mathbf{M} is dependent on the mode frequency ω , Eq. (31) is solved iteratively in conjunction with the FPD equation (24) by the following steps:

- (1) An initial guess, $\omega^{(0)}$, is chosen in \mathbf{M} to obtain $\Omega(\lambda)$ in Eq. (31) by making use of the QR decomposition technique (a matrix can be written as the product of an orthogonal matrix Q and an upper triangular matrix R);³³
- (2) The inverse power method is adopted to obtain \mathbf{A} and $\chi(k, \lambda)$;
- (3) $\chi(k, \lambda)$ is substituted into Eqs. (27) and (28) for calculating $\bar{L}_1(\lambda)$ and $\bar{L}_2(\lambda)$;
- (4) Use is made of the shooting method to solve Eq. (24) for the global eigenvalue $\Omega^{(1)}$;
- (5) $\Omega^{(1)}$ is substituted into Eq. (20) to obtain $\omega^{(1)}$;
- (6) Steps (1)–(5) are repeated (using $\omega^{(i)}$ to acquire $\omega^{(i+1)}$) till the convergence condition $|1 - \omega^{(i+1)}/\omega^{(i)}| < 10^{-4}$ is satisfied. The corresponding convergence condition for wave functions $|\varphi_0(x)|$ [the wave function in (x, l) representation for $l = 0$] is found to be $|1 - |\varphi_0(x)|^{(i+1)}/|\varphi_0(x)|^{(i)}| < 5 \times 10^{-4}$.

The machine and physical parameters are chosen as follows: $R = 1.65$ m, $a = 0.4$ m, $T_{e0} = 250$ eV, $B = 1.35$ T, $\hat{s} = 1$, $q_0 = 1$, $\eta_{i0} = 0$, $\eta_{e0} = 1$, $L_{n0}/R = 0.1$, $\varepsilon(r_j) = 0.1$, $\tau_{e0} = 10$, $r_j/a = 0.41$, and $k_{\vartheta} \rho_{s0} = 0.316$ corresponding to the toroidal mode number $n = -44$ for easier comparison with the results in Ref. 4.

In Figs. 1(a)–1(d), the ballooning space wave function $\chi(k, \lambda)$ in Eq. (23) is plotted versus k for $\lambda = 0, \pi/4, \pi/2$, and $-\pi/2$ (with $N = 10$); the blue (red) line denotes the real (imaginary) part. The

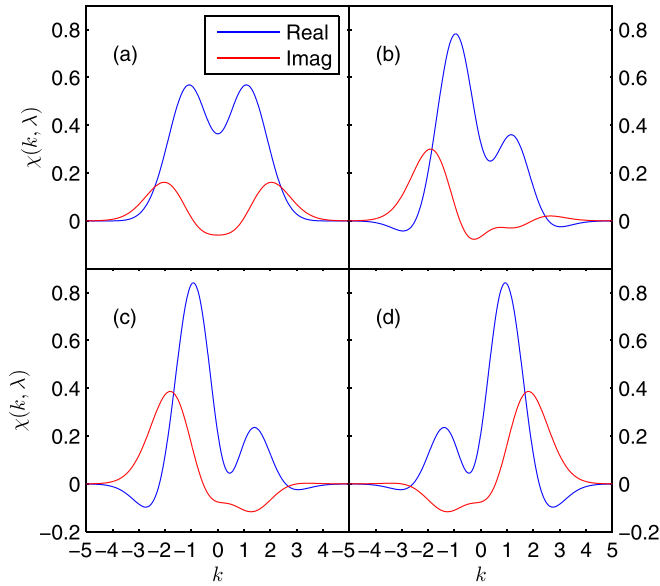


FIG. 1. The real (blue line) and imaginary (red line) parts of ballooning wave functions $\chi(k, \lambda)$ versus k obtained from Eq. (23) for (a) $\lambda = 0$; (b) $\lambda = \pi/4$; (c) $\lambda = \pi/2$; and (d) $\lambda = -\pi/2$. The physical parameters are $k_\theta \rho_{s0} = 0.316$, $\hat{s} = 1$, $q_0 = 1$, $\eta_{i0} = 0$, $\eta_{e0} = 1$, $L_{r0}/R = 0.1$, and $n = -44$.

dual peak structure of the wave function in Fig. 1(a) with $\lambda = 0$ is found to be qualitatively similar to that of 1D TEM [e.g., Fig. 2(a) in Ref. 5], implying that both the ballooning equations have similar potential structures. The corresponding local eigenvalues are listed in Table I. The local eigenvalue for 1D TEM at $\lambda = 0$, $\omega(\lambda = 0)/\omega_{*e0} = 0.429 + 0.250i$, seems close to the data shown in Fig. 2 of Ref. 4.

In Figs. 2(a)–2(d), the ballooning wave function $\chi(k, \lambda)$ of the last iteration, solved from Eqs. (23) and (24), is plotted versus k for $\lambda = 0, \pi/4, \pi/2$, and $-\pi/2$ (with $N = 10$); the blue and red lines denote the real and imaginary parts. In contrast to Fig. 1, the dual peak structure disappears. It suggests that the second dimension does have non-trivial effects on the potential structure via the mode frequency. Not surprisingly, the local eigenvalues decrease with the decreasing energy of the standing wave, as listed in Table I. The global eigenvalue is iteratively calculated to be $\omega/\omega_{*e0} = 0.354 + 0.174i$.

The obtained FPD $\psi(\lambda)$ is displayed in Fig. 3 with the same parameters as in Fig. 1. The solid lines (blue is the real part and red is the imaginary part) stand for the numerical solution obtained from Eq. (24) after 21 iterations. Two cases are studied for getting FPD. For case A, the pure numerical results of $\Omega(\lambda)$,

TABLE I. The local eigenvalues corresponding to the ballooning wave functions as displayed in Figs. 1(a)–1(d) and 2(a)–2(d), respectively.

λ	$\omega(\lambda)/\omega_{*e0}$ (1D TEM)	$\omega(\lambda)/\omega_{*e0}$ (the last iteration)
0	$0.429 + 0.250i$	$0.372 + 0.191i$
$\pi/4$	$0.432 + 0.243i$	$0.370 + 0.188i$
$\pm \pi/2$	$0.446 + 0.227i$	$0.368 + 0.184i$

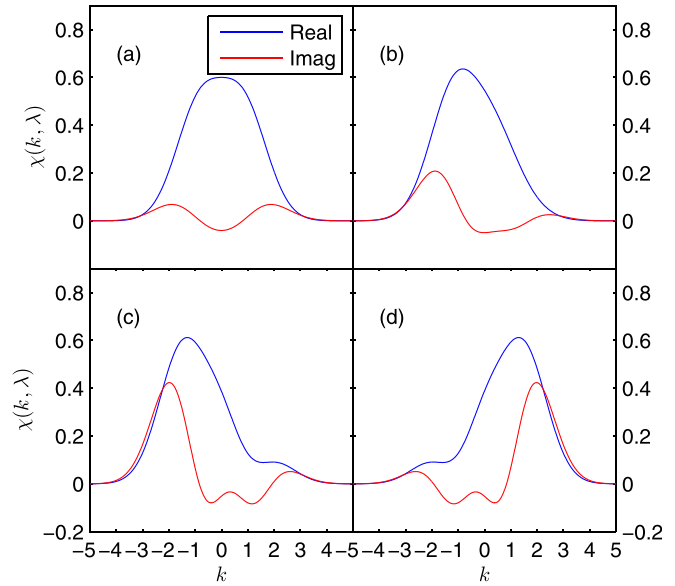


FIG. 2. The real (blue line) and imaginary (red line) parts of ballooning wave functions $\chi(k, \lambda)$ versus k calculated iteratively from Eqs. (23) and (24) for (a) $\lambda = 0$; (b) $\lambda = \pi/4$; (c) $\lambda = \pi/2$; and (d) $\lambda = -\pi/2$. The physical parameters are the same as in Fig. 1.

$\bar{L}_1(\lambda)$, and $\bar{L}_2(\lambda)$ are used exactly in the same way as in Ref. 18 (It will be used throughout this paper unless otherwise mentioned.), marked by the solid line in Fig. 3. For case B (dotted-dashed lines in Fig. 3), the approximation $\Omega(\lambda) \approx \Omega_0 + \Omega_1 \cos \lambda$ is

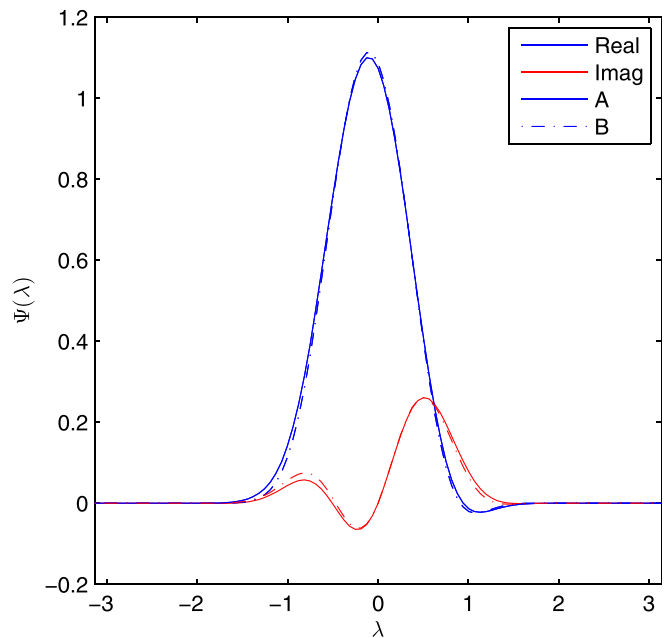


FIG. 3. The real (blue line) and imaginary (red line) parts of FPD $\psi(\lambda)$ versus λ . Case A (solid lines): the numerical results of $\Omega(\lambda)$, $\bar{L}_1(\lambda)$, and $\bar{L}_2(\lambda)$ are used; case B (dotted-dashed lines): $\Omega(\lambda)$ is expanded up to the first cosine harmonics.

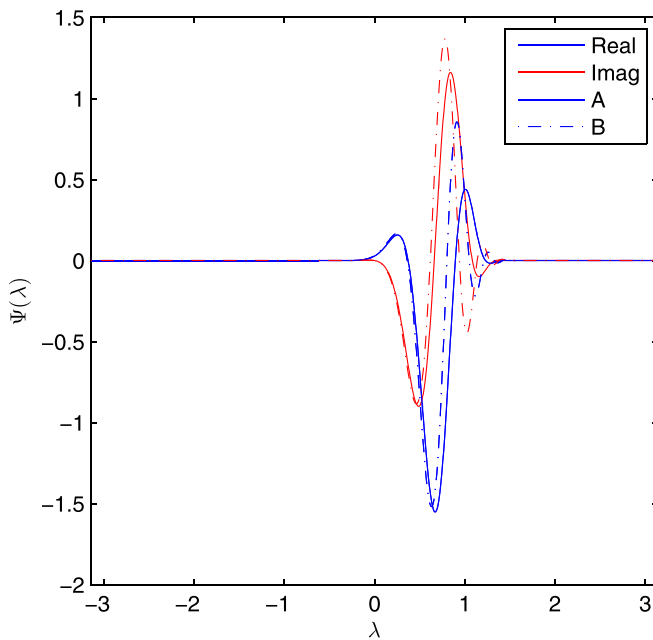


FIG. 4. The real (blue line) and imaginary (red line) parts of FPD $\psi(\lambda)$ versus λ for the kinetic ITG model. Cases A and B are the same as in Fig. 3.

adopted. Such an approximation is likely to be plausible for TEM, because the trapped electrons reside outboard in an up-down symmetric system. As a result, the peak deviation of $\psi(\lambda)$ is nearly zero, and good agreement is seen for the two cases that yield very close global eigenvalues. For the kinetic ITG model,¹⁸ the FPD $\psi(\lambda)$ for the abovementioned two cases is shown in Fig. 4. It is seen that the agreement of $\psi(\lambda)$ between the two is NOT as good as for TEM, because the peak deviation is relatively large for the parameters we have explored so far, while the global eigenvalues are still close enough.

The ballooning wave function $\chi(k, \lambda)$ and FPD $\psi(\lambda)$ will be used to calculate the natural boundary condition

$d \ln \varphi_l(x)/dx|_{x=x_{\pm}}$ for eigenvalue simulation by making use of Eq. (5), where x_{\pm} stands for outer-inner boundary.

In Fig. 5, the numeric 2D mode structure is shown via the contour plot of $\text{Re}[\varphi_n(r, \vartheta, 0)]$. The close-up view of Fig. 5(a) is shown in Fig. 5(b) for the detailed mode structure. The radial position is determined by the mapping $(1 + x/m\hat{s})(r_j/a)$. At first sight, the mode structure in Fig. 5(a) looks, largely, up-down symmetric. It is to be expected since the driving force arises from trapped electron population that is up-down symmetric in a symmetric equilibrium. However, a weakly asymmetric fine structure is identified in Fig. 5(b). Such an asymmetry would induce a finite residual Reynolds stress to drive the zonal flows. Using Fig. 5, we estimate that the radial correlation length is more than two times larger than the poloidal one; this is a manifestation of the toroidal coupling. In contrast to Fig. 5(a) for TEM, the 2D kinetic ITG mode in Fig. 3 of Ref. 18 appears more tilted and, likely, yields stronger Reynolds stress for the same turbulence level.

IV. SUMMARY

The present paper begins with solving the electron drift kinetic equation in physical space for non-adiabatic trapped electrons to the lowest order of $|\omega/\omega_{be}| < 1$, where ω_{be} is the electron bounce frequency. The 2D non-adiabatic density response of trapped electrons, obtained by integrating over velocity space, is then transformed into the 2D ballooning space.²⁷ The passing electrons are assumed to be adiabatic, and the effect of trapped ions is neglected. The quasi-neutrality condition, equating the density response from electrons and passing ions (developed in Ref. 18), yields the appropriate ballooning space mode equation describing the collisionless weakly up-down asymmetric TEM [see full form Eqs. (19) and (20) and the WABT form Eqs. (23)–(29)].

An iterative method is adopted to solve the 2D system for the WABT form. The ballooning equation is solved by making use of a spectral method based on Weber–Hermite functions, while the higher order equation is solved by a shooting method. The parameter set is chosen for a typical L-mode which is the same

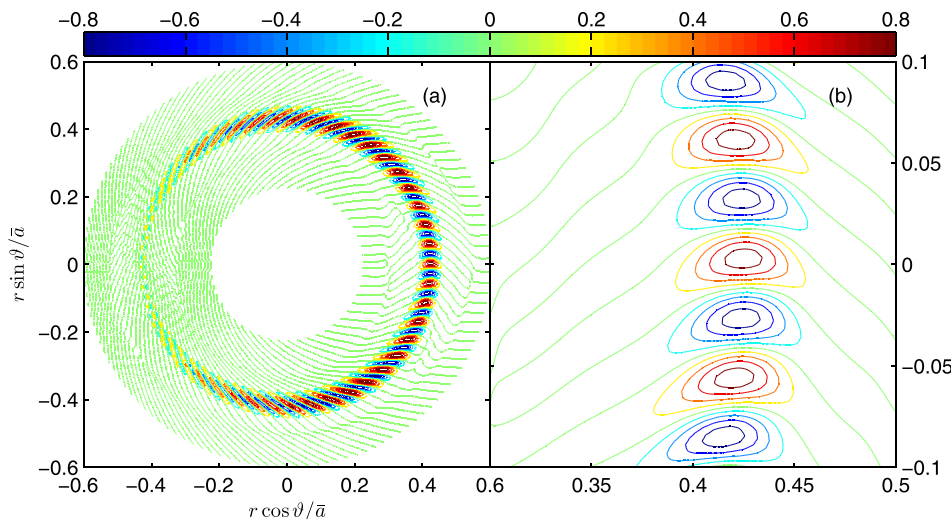


FIG. 5. Level contours of the real parts of the 2D mode structure on a poloidal cross section; (b) is the close-up view of (a).

as in Ref. 4. Both the global eigenvalue and wave function in physical space are proven to be convergent.

The eigenvalue ($\omega/\omega_{*e0} = 0.354 + 0.174i$) is quite different from what would pertain in a conventional 1D ballooning approach for $\lambda = 0$ ($0.429 + 0.250i$). It strongly suggests that the 2D theory is necessary for more accurate eigenvalues. More importantly, the 2D theory provides a 2D mode structure in physical space. Such knowledge is required for the natural boundary condition of simulation and in the calculation of Reynolds stress and group velocity for the zonal flow–drift wave system (to be presented elsewhere).

A numeric 2D mode structure is presented graphically in Fig. 5. Two features stand out: (1) the mode structure is weakly up-down asymmetric and (2) the ratio of the radial/poloidal correlation lengths is greater than 2; a fact deeply significant to the transport caused by TEM. The explicit calculations of Reynolds stress and group velocity, induced by the weakly up-down asymmetric TEM model, will be discussed and compared with the kinetic ITG model in future work.

Finally, we would like to mention a recently published alternative approach, based on the “Fourier-ballooning representation,” to construct a 2D ballooning theory³⁴ for the ITG mode. We hope that the two approaches will be complementary in advancing the physics of 2D micro-turbulence in tokamaks.

ACKNOWLEDGMENTS

This research was supported by the Key Research Program of Frontier Sciences CAS (QYZDB-SSWSYS004), National Magnetic Confinement Fusion Energy Research Project (Nos. 2014GB124004, 2015GB104004, and 2015GB111003), National Natural Science Foundation of China (Nos. NSFC-11575185, 11575186, 11705050, and 11775067), U.S. Department of Energy under Grant No. DE-FG02-04ER-54742, Foundation of Sichuan University of Science and Engineering under Grant No. 2016RCL21, Scientific Research Fund of the Sichuan Provincial Education Department under Grant No. 17ZA0281, and Sichuan University of Science and Engineering High Performance Computing Center for providing computation.

APPENDIX A: THE TRAPPED ELECTRON NON-ADIABATIC DENSITY RESPONSE FOR LARGE BOUNCE FREQUENCY

For large bounce frequency ($\omega_{be} > \omega$), the distribution function $h_n(r, \vartheta; v_{\parallel}, v_{\perp})$ of Eq. (1) can be expanded perturbatively

$$h_n(r, \vartheta; v_{\parallel}, v_{\perp}) \approx h_n^{(0)}(r, \vartheta; v_{\parallel}, v_{\perp}) + h_n^{(1)}(r, \vartheta; v_{\parallel}, v_{\perp}). \quad (\text{A1})$$

The lowest order (in ω/ω_{be}) equation is

$$\mathbf{b} \cdot \nabla h_n^{(0)}(r, \vartheta; v_{\parallel}, v_{\perp}) = \left(\frac{\partial}{\partial \vartheta} + inq(r) \right) h_n^{(0)}(r, \vartheta; v_{\parallel}, v_{\perp}) = 0. \quad (\text{A2})$$

The solution of Eq. (A2) can be put in the following form:

$$h_n^{(0)}(r, \vartheta; v_{\parallel}, v_{\perp}) = \bar{h}_n(r; v_{\parallel}, v_{\perp}) e^{-inq(r)\vartheta}, \quad (\text{A3})$$

where $\bar{h}_n(r; v_{\parallel}, v_{\perp})$ is to be determined by the following steps:

Multiplying the first order equation of Eq. (1)

$$\begin{aligned} (\omega - \hat{\omega}_{de}) \bar{h}_n(r; v_{\parallel}, v_{\perp}) e^{-inq(r)\vartheta} + iv_{\parallel} \mathbf{b} \cdot \nabla h_n^{(1)}(r, \vartheta; v_{\parallel}, v_{\perp}) \\ = -F_M(\omega - \hat{\omega}_{*T}) \varphi_n(r, \vartheta) \end{aligned} \quad (\text{A4})$$

by $e^{inq(r)\vartheta}/v_{\parallel}$ and integrating over ϑ to annihilate $h_n^{(1)}$ yields the equation for $\bar{h}_n(r; v_{\parallel}, v_{\perp})$

$$\begin{aligned} \oint d\vartheta \frac{1}{v_{\parallel}} e^{inq(r)\vartheta} (\omega - \hat{\omega}_{de}) \bar{h}_n(r; v_{\parallel}, v_{\perp}) e^{-inq(r)\vartheta} \\ = -F_M(\omega - \hat{\omega}_{*T}) \oint d\vartheta \frac{1}{v_{\parallel}} e^{inq(r)\vartheta} \varphi_n(r, \vartheta). \end{aligned} \quad (\text{A5})$$

Explicitly, the second term (proportional to $\hat{\omega}_{de}$) on the LHS of Eq. (A5) is

$$\begin{aligned} \hat{\omega}_{de} \bar{h}_n(r; v_{\parallel}, v_{\perp}) e^{-inq(r)\vartheta} = \frac{2iT_e}{eBR} \left(\hat{v}_{\parallel}^2 + \frac{1}{2} \hat{v}_{\perp}^2 \right) e^{-inq(r)\vartheta} \\ \times \left[\sin \vartheta \left(\frac{\partial}{\partial r} - in\vartheta \frac{dq(r)}{dr} \right) \right. \\ \left. - \frac{\cos \vartheta}{r} inq(r) \right] \bar{h}_n(r; v_{\parallel}, v_{\perp}). \end{aligned} \quad (\text{A6})$$

Since the radial correlation length is much longer than the poloidal one (see Fig. 5) for ballooning type modes, $\partial \bar{h}_n / \partial r$ can be neglected compared to $nq(r) \bar{h}_n / r$. Equation (A6), then, is approximated by

$$\begin{aligned} \hat{\omega}_{de} \bar{h}_n(r; v_{\parallel}, v_{\perp}) e^{-inq(r)\vartheta} \approx \frac{2T_e nq(r)}{eBR r} \left(\hat{v}_{\parallel}^2 + \frac{1}{2} \hat{v}_{\perp}^2 \right) \\ \times \left(\vartheta \sin \vartheta \frac{r}{q(r)} \frac{dq(r)}{dr} + \cos \vartheta \right) \\ \times \bar{h}_n(r; v_{\parallel}, v_{\perp}) e^{-inq(r)\vartheta}. \end{aligned} \quad (\text{A7})$$

For the trapped electron, $\hat{v}_{\parallel}^2 \ll \hat{v}_{\perp}^2$, and Eq. (A7) reduces to

$$\hat{\omega}_{de} \bar{h}_n(r; v_{\parallel}, v_{\perp}) e^{-inq(r)\vartheta} \approx \omega_{de} \hat{v}_{\perp}^2 \bar{h}_n(r; v_{\parallel}, v_{\perp}) e^{-inq(r)\vartheta}, \quad (\text{A8})$$

where

$$\omega_{de} \equiv \frac{T_e}{eBR} \frac{nq(r)}{r} \left(\vartheta \sin \vartheta \frac{r}{q(r)} \frac{dq(r)}{dr} + \cos \vartheta \right). \quad (\text{A9})$$

Substituting Eq. (A8) into Eq. (A5), one obtains

$$\bar{h}_n(r; v_{\parallel}, v_{\perp}) = -F_M \frac{\omega - \hat{\omega}_{*T}}{\omega - \langle \omega_{de} \rangle \hat{v}_{\perp}^2} \langle e^{inq(r)\vartheta} \varphi_n(r, \vartheta) \rangle, \quad (\text{A10})$$

where

$$\langle \dots \rangle \equiv \frac{\oint d\vartheta \frac{1}{v_{\parallel}} (\dots)}{\oint d\vartheta \frac{1}{v_{\parallel}}} = \frac{1}{4K(\kappa)} \oint \frac{d\vartheta}{\sqrt{\kappa^2 - \sin^2 \frac{\vartheta}{2}}} (\dots), \quad (\text{A11})$$

$$\langle \omega_{de} \rangle = \frac{T_e}{eBR} \frac{nq(r)}{r} \left(\frac{r}{r_j} \frac{q(r_j)}{q(r)} \hat{s} \langle \vartheta \sin \vartheta \rangle + \langle \cos \vartheta \rangle \right), \quad (\text{A12})$$

$$\langle \vartheta \sin \vartheta \rangle = 4 \left[\frac{E(\kappa)}{K(\kappa)} - (1 - \kappa^2) \right], \quad (\text{A13})$$

$$\langle \cos \vartheta \rangle = \frac{2E(\kappa)}{K(\kappa)} - 1, \quad (\text{A14})$$

$\hat{s} \equiv (r_j/q(r_j))(dq/dr)|_{r_j}$ is the magnetic shear and $K(\kappa)$ and $E(\kappa)$ are the complete elliptic integrals of the first and second kind, respectively.

Integrating $\bar{h}_n(r; v_{\parallel}, v_{\perp})$ over velocity space yields the dimensionless non-adiabatic density response of trapped electrons

$$\hat{n}_{te}(r, \vartheta) = -e^{-inq(r)\vartheta} \int dv^3 F_M \frac{\omega - \hat{\omega}_{*T}}{\omega - \langle \omega_{de} \rangle \hat{v}^2} \langle e^{inq(r)\vartheta} \varphi_n(r, \vartheta) \rangle. \quad (\text{A15})$$

APPENDIX B: SOME DEFINITIONS IN THE HIGHER ORDER EQUATION

There are four coefficients in Eqs. (27) and (28), namely, $\frac{dK(\kappa, \lambda)}{d\lambda}|_{\lambda=0}$, $\frac{d^2K(\kappa, \lambda)}{d\lambda^2}|_{\lambda=0}$, $\frac{dg(\kappa, \lambda)}{d\lambda}|_{\lambda=0}$, and $\frac{d^2g(\kappa, \lambda)}{d\lambda^2}|_{\lambda=0}$. The first two are given by Eqs. (23) and (24) of Ref. 18. The latter two are as follows:

$$\frac{dg(\kappa, \lambda)}{d\lambda}\Big|_{\lambda=0} = -\frac{1}{(1+\tau_{e0})} \sqrt{\frac{2\varepsilon_0}{\pi}} \frac{\omega}{\omega_{*e0}} \hat{I}(\varsigma_{e0}) \frac{d\tau_e}{d\lambda} + \sqrt{\frac{1}{2\pi\varepsilon_0}} \frac{\omega}{\omega_{*e0}} \hat{I}(\varsigma_{e0}) \frac{d\varepsilon_0}{d\lambda} + \sqrt{\frac{2\varepsilon_0}{\pi}} \frac{\omega}{\omega_{*e0}} \frac{d\hat{I}(\varsigma_e)}{d\lambda}, \quad (\text{B1})$$

$$\begin{aligned} \frac{d^2g(\kappa, \lambda)}{d\lambda^2}\Big|_{\lambda=0} &= -\frac{1}{(1+\tau_{e0})} \sqrt{\frac{2\varepsilon_0}{\pi}} \frac{\omega}{\omega_{*e0}} \hat{I}(\varsigma_{e0}) \frac{d^2\tau_e}{d\lambda^2} + \sqrt{\frac{1}{2\pi\varepsilon_0}} \frac{\omega}{\omega_{*e0}} \hat{I}(\varsigma_{e0}) \frac{d^2\varepsilon(r)}{d\lambda^2} + \sqrt{\frac{2\varepsilon_0}{\pi}} \frac{\omega}{\omega_{*e0}} \frac{d^2\hat{I}(\varsigma_e)}{d\lambda^2} \\ &+ \frac{2}{(1+\tau_{e0})^2} \sqrt{\frac{2\varepsilon_0}{\pi}} \frac{\omega}{\omega_{*e0}} \hat{I}(\varsigma_{e0}) \left(\frac{d\tau_e}{d\lambda}\right)^2 - \frac{1}{2\varepsilon_0} \sqrt{\frac{1}{2\pi\varepsilon_0}} \frac{\omega}{\omega_{*e0}} \hat{I}(\varsigma_{e0}) \left(\frac{d\varepsilon(r)}{d\lambda}\right)^2 \\ &- \frac{1}{(1+\tau_{e0})} \sqrt{\frac{2}{\pi\varepsilon_0}} \frac{\omega}{\omega_{*e0}} \hat{I}(\varsigma_{e0}) \frac{d\varepsilon(r)}{d\lambda} \frac{d\tau_e}{d\lambda} - \frac{2}{(1+\tau_{e0})} \sqrt{\frac{2\varepsilon_0}{\pi}} \frac{\omega}{\omega_{*e0}} \frac{d\hat{I}(\varsigma_e)}{d\lambda} \frac{d\tau_e}{d\lambda} + \sqrt{\frac{2}{\pi\varepsilon_0}} \frac{\omega}{\omega_{*e0}} \frac{d\hat{I}(\varsigma_e)}{d\lambda} \frac{d\varepsilon(r)}{d\lambda}, \end{aligned} \quad (\text{B2})$$

where $\varepsilon_0 = r_j/R$,

$$\frac{d\varepsilon(r)}{d\lambda} = \frac{r_0}{\hat{s}R}, \quad \frac{d^2\varepsilon(r)}{d\lambda^2} = 0, \quad (\text{B3})$$

$$\frac{d\tau_e}{d\lambda} = \tau_{e0}(t_{T_i} - t_{T_e}), \quad \frac{d^2\tau_e}{d\lambda^2} = 2\tau_{e0}t_{T_i}(t_{T_i} - t_{T_e}), \quad (\text{B4})$$

$$\frac{\omega}{\omega_{*e0}} \frac{d\hat{I}(\varsigma_{e0})}{d\lambda} = \frac{2}{\varsigma_{e0}} \frac{d\varsigma_e}{d\lambda} \hat{I}(\varsigma_{e0}) + \sqrt{\pi}\varsigma_{e0}^2 C_1, \quad (\text{B5})$$

$$\frac{\omega}{\omega_{*e0}} \frac{d^2\hat{I}(\varsigma_e)}{d\lambda^2} = 2 \left[\left(\frac{1}{\varsigma_{e0}} \frac{d\varsigma_e}{d\lambda} \right)^2 + \frac{1}{\varsigma_{e0}} \frac{d^2\varsigma_e}{d\lambda^2} \right] \frac{\omega}{\omega_{*e0}} \hat{I}(\varsigma_{e0}) + 4\sqrt{\pi}\varsigma_{e0} \frac{d\varsigma_e}{d\lambda} C_1 + \sqrt{\pi}\varsigma_{e0}^2 C_2, \quad (\text{B6})$$

$$\begin{aligned} C_1 &\equiv \left(\frac{d\varsigma_e}{d\lambda} Z(\varsigma_{e0}) + \varsigma_{e0} \frac{dZ(\varsigma_e)}{d\lambda} \right) \left(\frac{\omega}{\omega_{*e0}} - 1 \right) - \frac{dA_{\omega_{*e}}}{d\lambda} (1 + \varsigma_{e0} Z(\varsigma_{e0})) + \frac{d\eta_e}{d\lambda} \left[1 - \varsigma_{e0}^2 + \varsigma_{e0} Z(\varsigma_{e0}) \left(\frac{3}{2} - \varsigma_{e0}^2 \right) \right] \\ &+ \eta_{e0} \frac{dA_{\omega_{*e}}}{d\lambda} \left[1 - \varsigma_{e0}^2 + \varsigma_{e0} Z(\varsigma_{e0}) \left(\frac{3}{2} - \varsigma_{e0}^2 \right) \right] + \eta_{e0} \left[-2\varsigma_{e0} \frac{d\varsigma_e}{d\lambda} + \frac{dZ(\varsigma_e)}{d\lambda} \left(\frac{3}{2}\varsigma_{e0} - \varsigma_{e0}^3 \right) + Z(\varsigma_{e0}) \left(\frac{3}{2} - 3\varsigma_{e0}^2 \right) \frac{d\varsigma_e}{d\lambda} \right], \end{aligned} \quad (\text{B7})$$

$$\begin{aligned} C_2 &\equiv \left(\frac{d^2\varsigma_e}{d\lambda^2} Z(\varsigma_e) + 2 \frac{d\varsigma_e}{d\lambda} \frac{dZ(\varsigma_e)}{d\lambda} + \varsigma_{e0} \frac{d^2Z(\varsigma_e)}{d\lambda^2} \right) \left(\frac{\omega}{\omega_{*e0}} - 1 \right) - 2 \frac{dA_{\omega_{*e}}}{d\lambda} \left(\frac{d\varsigma_e}{d\lambda} Z(\varsigma_e) + \varsigma_{e0} \frac{dZ(\varsigma_e)}{d\lambda} \right) \\ &+ 2 \frac{d\eta_e}{d\lambda} \frac{dA_{\omega_{*e}}}{d\lambda} \left[1 - \varsigma_{e0}^2 + \varsigma_{e0} Z(\varsigma_e) \left(\frac{3}{2} - \varsigma_{e0}^2 \right) \right] + 2 \frac{d\eta_e}{d\lambda} \left[-2\varsigma_{e0} \frac{d\varsigma_e}{d\lambda} + \frac{dZ(\varsigma_e)}{d\lambda} \left(\frac{3}{2}\varsigma_{e0} - \varsigma_{e0}^3 \right) + Z(\varsigma_e) \left(\frac{3}{2} - 3\varsigma_{e0}^2 \right) \frac{d\varsigma_e}{d\lambda} \right] \\ &+ 2\eta_{e0} \frac{dA_{\omega_{*e}}}{d\lambda} \left[-2\varsigma_{e0} \frac{d\varsigma_e}{d\lambda} + \frac{dZ(\varsigma_e)}{d\lambda} \left(\frac{3}{2}\varsigma_{e0} - \varsigma_{e0}^3 \right) + Z(\varsigma_e) \left(\frac{3}{2} - 3\varsigma_{e0}^2 \right) \frac{d\varsigma_e}{d\lambda} \right] - (1 + \varsigma_{e0} Z(\varsigma_e)) \frac{d^2A_{\omega_{*e}}}{d\lambda^2} \\ &+ \eta_{e0} \left[-2(1 + 3\varsigma_{e0} Z(\varsigma_e)) \left(\frac{d\varsigma_e}{d\lambda} \right)^2 + \frac{d^2Z(\varsigma_e)}{d\lambda^2} \left(\frac{3}{2}\varsigma_{e0} - \varsigma_{e0}^3 \right) + 2 \frac{dZ(\varsigma_e)}{d\lambda} \left(\frac{3}{2} - 3\varsigma_{e0}^2 \right) \frac{d\varsigma_e}{d\lambda} - 2\varsigma_{e0} \frac{d^2\varsigma_e}{d\lambda^2} + Z(\varsigma_e) \left(\frac{3}{2} - 3\varsigma_{e0}^2 \right) \frac{d^2\varsigma_e}{d\lambda^2} \right] \\ &+ \eta_{e0} \frac{d^2A_{\omega_{*e}}}{d\lambda^2} \left[1 - \varsigma_{e0}^2 + \varsigma_{e0} Z(\varsigma_e) \left(\frac{3}{2} - \varsigma_{e0}^2 \right) \right] + \frac{d^2\eta_e}{d\lambda^2} \left[1 - \varsigma_{e0}^2 + \varsigma_{e0} Z(\varsigma_e) \left(\frac{3}{2} - \varsigma_{e0}^2 \right) \right], \end{aligned} \quad (\text{B8})$$

$$\frac{d\zeta_e}{d\lambda} = \frac{1}{2}\zeta_{e0} \left[t_{Te} - \left(1 - \frac{1}{\bar{s}}\right) \frac{\langle \cos \vartheta \rangle}{(\hat{s} \langle \vartheta \sin \vartheta \rangle + \langle \cos \vartheta \rangle)} \right], \quad (\text{B9})$$

$$\begin{aligned} \frac{d^2\zeta_e}{d\lambda^2} &= \frac{3}{4}\zeta_{e0} \left[t_{Te} - \left(1 - \frac{1}{\bar{s}}\right) \frac{\langle \cos \vartheta \rangle}{(\hat{s} \langle \vartheta \sin \vartheta \rangle + \langle \cos \vartheta \rangle)} \right]^2 \\ &+ \zeta_{e0} \frac{\langle \cos \vartheta \rangle}{(\hat{s} \langle \vartheta \sin \vartheta \rangle + \langle \cos \vartheta \rangle)} \left(1 - \frac{1}{\bar{s}}\right) \left(t_{Te} + \frac{1}{2\bar{s}} \right), \end{aligned} \quad (\text{B10})$$

$$\frac{dn_e}{d\lambda} = t_n \eta_{e0} (\eta_{e0} - 1), \quad \frac{d^2 n_e}{d\lambda^2} = 2\eta_{e0} t_n t_{Te} (\eta_{e0} - 1), \quad (\text{B11})$$

$$\frac{dA_{\omega_e}}{d\lambda} = \left(1 - \frac{1}{\bar{s}}\right) - t_n (\eta_{e0} - 1), \quad (\text{B12})$$

$$\frac{d^2 A_{\omega_e}}{d\lambda^2} = -2 \left[\frac{1}{\bar{s}} \left(1 - \frac{1}{\bar{s}}\right) + t_n (\eta_{e0} - 1) \left(1 - \frac{1}{\bar{s}}\right) + t_n^2 (\eta_{e0} - 1) \right], \quad (\text{B13})$$

$$\frac{dZ(\zeta_e)}{d\lambda} = -2 \frac{d\zeta_e}{d\lambda} (1 + \zeta_{e0} Z(\zeta_{e0})), \quad (\text{B14})$$

$$\begin{aligned} \frac{d^2 Z(\zeta_e)}{d\lambda^2} &= -2 \frac{d^2 \zeta_e}{d\lambda^2} (1 + \zeta_{e0} Z(\zeta_{e0})) \\ &- 2 \frac{d\zeta_e}{d\lambda} \left(\frac{d\zeta_e}{d\lambda} Z(\zeta_{e0}) + \zeta_{e0} \frac{dZ(\zeta_e)}{d\lambda} \right). \end{aligned} \quad (\text{B15})$$

REFERENCES

- ¹J. W. Connor and H. R. Wilson, *Plasma Phys. Controlled Fusion* **36**, 719 (1994).
- ²W. M. Tang, J. W. Connor, and R. J. Hastie, *Nucl. Fusion* **18**, 1089 (1978).
- ³W. M. Tang, J. W. Connor, and R. J. Hastie, *Nucl. Fusion* **20**, 1439 (1980).
- ⁴C. Z. Cheng and L. Chen, *Nucl. Fusion* **21**, 403 (1981).
- ⁵G. Rewoldt, W. M. Tang, and M. S. Chance, *Phys. Fluids* **25**, 480 (1982).
- ⁶G. Rewoldt and W. M. Tang, *Phys. Fluids B* **2**, 318 (1990).
- ⁷J. Q. Dong, S. M. Mahajan, and W. Horton, *Phys. Plasmas* **4**, 755 (1997).
- ⁸C. Z. Cheng and N. N. Gorelenkov, *Phys. Plasmas* **11**, 4784 (2004).
- ⁹H. Du, Z.-X. Wang, J. Q. Dong, and S. F. Liu, *Phys. Plasmas* **21**, 052101 (2014).
- ¹⁰N. Zhang, X. Y. Gong, J. Q. Dong, Q. H. Huang, L. Gong, and J. C. Li, *Phys. Plasmas* **23**, 042508 (2016).
- ¹¹Y. Shen, J. Q. Dong, A. P. Sun, H. P. Qu, G. M. Lu, Z. X. He, H. D. He, and L. F. Wang, *Plasma Phys. Controlled Fusion* **58**, 045028 (2016).
- ¹²Y. C. Lee and J. W. Van Dam, in *Proceedings of the Finite Beta Theory Workshop*, Varenna Summer School of Plasma Physics, Varenna, Italy, September 1977, edited by B. Coppi and B. Sadowski (U.S. Department of Energy, Office of Fusion Energy, Washington DC, 1979), Paper No. CONF-7709167, p. 93.
- ¹³J. W. Connor, R. J. Hastie, and J. B. Taylor, *Phys. Rev. Lett.* **40**, 396 (1978).
- ¹⁴A. H. Glasser, in *Proceedings of the Finite Beta Theory Workshop*, Varenna Summer School of Plasma Physics, Varenna, Italy, September 1977, edited by B. Coppi and B. Sadowski (U.S. Department of Energy, Office of Fusion Energy, Washington DC, 1979), Paper No. CONF-7709167, p. 55.
- ¹⁵F. Pegoraro and T. Schep, in *Seventh Conference on Plasma Physics and Controlled Nuclear Fusion Research*, Innsbruck, August 1978 (International Atomic Energy Agency, Vienna, 1979), Paper No. IAEA-CN-37/F-51, p. 1.
- ¹⁶Y. Z. Zhang and T. Xie, *Nucl. Fusion Plasma Phys.* **33**, 193 (2013) (in Chinese with English abstract).
- ¹⁷T. Xie, H. Qin, Y. Z. Zhang, and S. M. Mahajan, *Phys. Plasmas* **23**, 042514 (2016).
- ¹⁸T. Xie, Y. Z. Zhang, S. M. Mahajan, S. L. Hu, H. He, and Z. Y. Liu, *Phys. Plasmas* **24**, 102506 (2017).
- ¹⁹T. Xie, Y. Z. Zhang, S. M. Mahajan, Z. Y. Liu, and H. He, *Phys. Plasmas* **23**, 102313 (2016).
- ²⁰P. H. Diamond, S.-I. Itoh, K. Itoh, and T. S. Hahm, *Plasma Phys. Controlled Fusion* **47**, R35 (2005).
- ²¹A. Fujisawa, *Nucl. Fusion* **49**, 013001 (2009).
- ²²Y. Z. Zhang, Z. Y. Liu, T. Xie, S. M. Mahajan, and J. Liu, *Phys. Plasmas* **24**, 122304 (2017).
- ²³D. W. Ross and S. M. Mahajan, *Phys. Rev. Lett.* **40**, 324 (1978).
- ²⁴K. T. Tsang, P. J. Catto, J. C. Whitson, and J. Smith, *Phys. Rev. Lett.* **40**, 327 (1978).
- ²⁵L. D. Pearlstein and H. L. Berk, *Phys. Rev. Lett.* **23**, 220 (1969).
- ²⁶P. J. Catto, *Plasma Phys.* **20**, 719 (1978).
- ²⁷Y. Z. Zhang and S. M. Mahajan, *Phys. Lett. A* **157**, 133 (1991).
- ²⁸Y. Z. Zhang, S. M. Mahajan, and X. D. Zhang, *Phys. Fluids B* **4**, 2729 (1992).
- ²⁹D. Dickinson, C. M. Roach, J. M. Skipp, and H. R. Wilson, *Phys. Plasmas* **21**, 010702 (2014).
- ³⁰J. B. Taylor, H. R. Wilson, and J. W. Connor, *Plasma Phys. Controlled Fusion* **38**, 243 (1996).
- ³¹E. A. Frieman, G. Rewoldt, W. M. Tang, and A. H. Glasser, *Phys. Fluids* **23**, 1750 (1980).
- ³²G. Rewoldt, W. M. Tang, and R. J. Hastie, *Phys. Fluids* **30**, 807 (1987).
- ³³J. Stoer and R. Bulirsch, *Introduction to Numerical Analysis*, 2nd ed. (Springer-Verlag, New York, NY, 2002), Sect. 6.6, p. 370.
- ³⁴P. A. Abdoul, D. Dickinson, C. M. Roach, and H. R. Wilson, *Plasma Phys. Controlled Fusion* **60**, 025011 (2018).